Optics and Lasers in Engineering 204 (2026) 109884

Contents lists available at ScienceDirect

Optics and Lasers in Engineering

journal homepage: www.elsevier.com/locate/optlaseng

Light sheet hologram encoding using binary amplitude modulation with complex loss optimization

Juan Andrés González-Moncada *, Alejandro Velez-Zea, John Fredy Barrera-Ramírez

Grupo de Óptica y Fotónica, Instituto de Física, Facultad de Ciencias Exactas y Naturales, Universidad de Antioquia UdeA, Calle 70 No 52-21, Medellín, Colombia

ARTICLE INFO

Keywords:
Computer-generated holography
Binary amplitude modulation
Light sheets
Stochastic gradient descent optimization

ABSTRACT

We demonstrate, for the first time to our knowledge, the encoding and reconstruction of high-quality holographic light sheets using binary amplitude modulation. This is achieved using an optimization scheme with a complex-valued loss function that evaluates the error at a single plane to optimize the reconstruction of a continuous three-dimensional light field. The method is validated numerically and experimentally, demonstrating enhanced reconstruction quality across the entire light sheet compared to direct binarization. We further demonstrate that optimized binary light sheet holograms adequately reproduce both bidimensional and multiplane scenes within a wide range of distances from the hologram plane. These results demonstrate the viability of binary amplitude modulators for reproducing high-complexity structured light fields, lowering the barrier to entry for a broad range of applications.

1. Introduction

Since its invention in 1948 [1], holography has remained an attractive technique due to its ability to record and reproduce optical fields. Computer-generated holography (CGH) is a digital variant of holography first developed in the 1960s [2,3], in which holograms are synthesized numerically. These holograms can then be projected using spatial light modulators (SLMs), enabling a broad range of applications. In recent decades, advancements in computational capabilities and SLM technology have driven the rapid evolution of CGH [4]. Currently, CGH is a fundamental tool in many fields, including microscopy [5], metrology [6,7], security printing [8], particle manipulation [9], three-dimensional (3D) display technology [10], and optical data encryption [11–13], among others.

Despite significant progress, CGH still faces fundamental limitations that restrict its applicability. Crucially, SLMs cannot simultaneously control all properties of the optical field; instead, they are typically restricted to modulating either the phase or the amplitude of the field. Consequently, CGH is commonly categorized into phase-only holography (POH) and amplitude-only holography (AOH), each requiring specialized algorithms to achieve high-quality reconstructions using existing devices [14]. In this context, the emergence of high-resolution, high refresh rate, low-cost binary amplitude modulators, called digital micromirror devices (DMDs), has renewed interest in binary amplitude holograms (BAHs) [15–18], where amplitude is constrained to two levels and the hologram generation process must be adapted accordingly.

Hologram generation algorithms can be classified into iterative and non-iterative methods. Non-iterative methods enable fast, direct hologram generation that reproduces the intended optical field while maintaining noise within acceptable limits, often at the cost of additional technical limitations. For POH, these methods include error diffusion [19], codification algorithms [20], quadratic phase masks [21], and deep learning schemes that include specific experimental parameters into the hologram generation process to achieve improved reconstruction quality [22–24]. In the case of BAHs, usually a previously generated phase-only hologram or amplitude-only hologram is binarized using a range of non-iterative approaches, such as different binarization algorithms [25], error diffusion [26,27], and the use of specifically tailored carrier waves [26]. For BAHs, non-iterative methods also enable fast hologram generation but typically produce reconstructions of limited quality.

Iterative methods enhance reconstruction quality by progressively refining the hologram through repeated calculations of its output. In the case of BAH, iterative methods include the direct binary search (DBS) algorithm and its variants [28–31], as well as the significantly faster binary-stochastic gradient descent (B-SGD) method [32–34], which minimize a chosen loss function. Iterative methods generally yield

* Corresponding author.
E-mail address: juan.gonzalezm1@udea.edu.co (J.A. González-Moncada).

https://doi.org/10.1016/j.optlaseng.2026.109884
Received 8 February 2026; Received in revised form 15 April 2026; Accepted 13 May 2026
Available online 25 May 2026

higher-fidelity reconstructions than non-iterative techniques. However, they require a significantly higher computational cost.

Conventionally, iterative approaches based on loss function minimization employ metrics that consider only the reconstructed intensity at a single plane. These methods can be extended to 3D intensity control by using composite loss functions that analyze intensity at multiple planes [35–38]. However, this strategy requires propagating the hologram to each plane at every optimization step, causing the computational cost to scale with the number of planes considered. This scaling becomes particularly problematic when reproducing high-complexity structured optical fields over extended ranges along the direction of light propagation.

One particularly interesting example of these extended structured optical fields is frozen waves. Frozen waves are composed of non-diffracting beams, such as Bessel and Bessel–Gauss beams [39], which maintain their transverse profile during free-space propagation. The superposition of these beams produces constructive and destructive interference along the propagation direction, resulting in a static longitudinal intensity profile. These fields exhibit self-healing and attenuation-resistant behavior [40], and have proven valuable for particle manipulation [41,42], where the high modulation rates of digital micromirror devices (DMDs) could be especially advantageous. Despite these benefits, frozen waves are challenging to encode into holograms using optimization approaches based on intensity-only loss functions. This is because evaluating the loss requires sampling numerous propagation planes, leading to substantial computational cost. Moreover, intensity-based optimization makes it difficult to fully exploit the flexibility of frozen waves for engineering fields with specific angular momentum [43] or polarization [44,45] properties.

More recently, frozen waves have been proposed for 3D scene projection by generating a sequence of slices reconstructed on planes perpendicular to the hologram plane [46]. These slices are known as holographic light sheets, and have seen significant advances in recent years, including the generation of curved light sheets [47], implementations based on orthogonal communication modes [48], and approaches that leverage deep learning techniques [49]. Compared to conventional reconstructions using slices parallel to the hologram, holographic light sheets enable finer and more uniform sampling of 3D scenes, as parallel slicing requires larger and non-uniform separation to mitigate crosstalk. In addition, holographic light sheets have been applied to microscopy [50,51], and metrology under turbulent conditions [52], where the capabilities of DMDs could be effectively exploited. However, reproducing frozen waves and holographic light sheets while preserving their desirable properties through intensity-loss minimization remains computationally impractical.

An alternative approach to achieve 3D intensity control entails complex modulation of the optical field, since reproducing the complex field at a single plane is sufficient to recover the entire 3D distribution [53]. In the case of BAHs, proposed complex modulation strategies include optimization schemes based on the DBS algorithm [30], Lee holography [54], and grouping multiple pixels into superpixels to encode complex values [55]. However, each of these approaches presents significant drawbacks: the DBS algorithm is computationally prohibitive, Lee holography requires scene-dependent parameter tuning, and superpixel encoding incurs substantial resolution loss. Recently, a study demonstrated the effectiveness of B-SGD with complex loss functions to reproduce a variety of 3D scenes using BAHs [34]; however, the demonstrated examples relied on conventional layer-based holography, which still demands a large separation between slices.

Given the above points, we propose an optimization scheme in the Fresnel domain that enables the encoding of arbitrary complex optical fields into BAHs by minimizing a complex-valued loss function evaluated at a single propagation plane. This significantly reduces the computational cost associated with encoding scenes with large axial extent into BAHs, which in conventional approaches typically requires optimizing intensity-based loss functions across multiple planes.

Then, we apply the proposed method to encode scenes composed of holographic light sheets into BAHs. The resulting holograms are reconstructed to demonstrate the capability of reproducing closely spaced light sheets, with inter-sheet separations that lead to significant crosstalk in conventional layer-based holography. We also evaluate the performance of the method under various conditions, identifying limitations associated with the available dynamic range and the finite hologram size.

Finally, we experimentally validate the proposed approach by implementing, to the best of our knowledge, the first experimental DMD-based scheme for holographic light-sheet projection. The results show improved performance compared with the direct binarization of amplitude light-sheet holograms and highlight the potential of this approach to lower the barrier to entry for several applications of light-sheet holography.

2. Methodology

The fundamental building blocks of frozen waves are nondiffracting waves, which maintain their transverse intensity profile as they propagate through free space. A representative example of such waves is the Bessel beam, given by

$$\psi(\rho,\phi,z,t) = e^{i\omega t} e^{i\nu\phi} J_\nu(k_\rho \rho) e^{ik_z z}, \tag{1}$$

where (ρ,ϕ,z) denote cylindrical coordinates, t is time, ω is the angular frequency, ν is the order of the Bessel beam, J_ν is a Bessel function of the first kind, and k_ρ and k_z are the radial and longitudinal components of the wavevector of magnitude $k = 2\pi/\lambda$, respectively. Frozen waves are defined as superpositions of copropagating Bessel beams with equal frequency [39], which interfere constructively and destructively to produce a static intensity profile along the longitudinal direction, as depicted in Fig. 1.

A zero-order frozen wave is given by

$$\Psi(\rho,z,t) = e^{i\omega t} \sum_{n=-N}^{N} A_n J_0(k_{\rho,n}\rho) e^{ik_{z,n} z}, \tag{2}$$

where $2N+1$ is the number of superposed Bessel beams, A_n are the coefficients, and $k_{\rho,n}$ and $k_{z,n}$ are the respective components of the wavevector of each Bessel beam. These parameters must be chosen to reproduce a desired intensity profile along $\rho = 0$ in the range defined by $0 \le z \le L$, where L is the extension of the frozen wave. A hologram $H(x,y)$ of the frozen wave is obtained by evaluating the complex field $\Psi(\rho,z,t)$ at the hologram plane $z = 0$, as illustrated in Fig. 1. Given an intensity profile $|F(z)|^2$, Zamboni-Rached [39] proposed setting the longitudinal components $k_{z,n}$ as follows:

$$k_{z,n} = Q + \frac{2\pi n}{L}, \tag{3}$$

where Q is a central longitudinal wavevector selected according to the experimental parameters. A detailed explanation of the parameters involved in determining the optimal value of Q can be found in Ref [46]. The choice of $k_{z,n}$ determines the number $2N+1$ of superposed Bessel beams according to the inequality

$$k_{z,N} \le k. \tag{4}$$

Specifically, this condition bounds the number N as

$$N = \left\lfloor (k-Q)\frac{L}{2\pi} \right\rfloor, \tag{5}$$

where the operator $\lfloor x \rfloor$ returns the greatest integer less than or equal to its argument. In turn, the radial component of each Bessel beam is given by

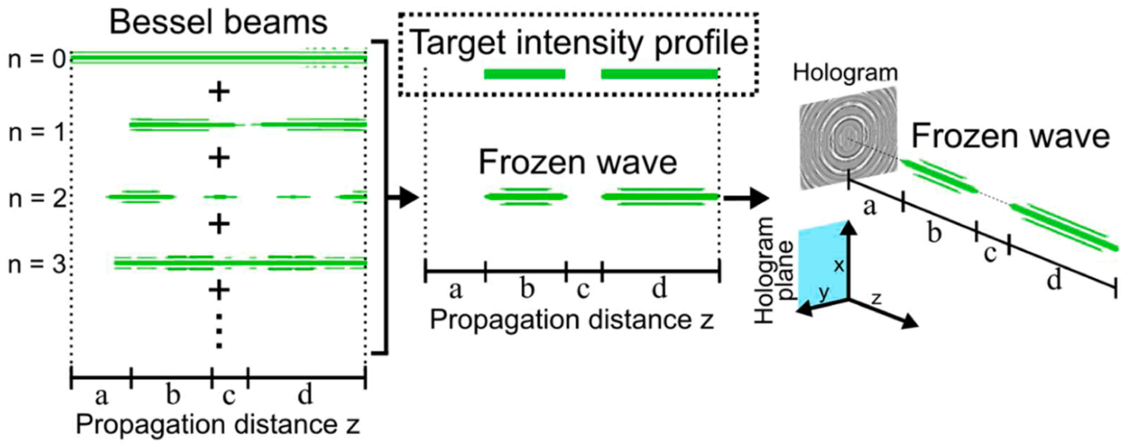

Fig. 1. Generation of frozen waves through superposition of Bessel beams. a, b, c, d: propagation distances.

$$k_{\rho,n} = \sqrt{k^2 - k_{z,n}^2}. \tag{6}$$

Correspondingly, the coefficient of each constituent beam in the superposition is determined by

$$A_n = \frac{1}{L}\int_0^L F(z) e^{-\frac{i2\pi nz}{L}} dz. \tag{7}$$

Eq. (2), together with the parameters set by Eqs. (3)-(7), describes a frozen wave that reproduces the target intensity profile along the longitudinal axis and generates periodic copies of this profile with a spatial period of L [56]. This method can also be applied to the reproduction of target scenes as depicted in Fig. 2.a) by rasterizing the target scene row by row to obtain several intensity profiles parallel to the light propagation axis. These intensity profiles are used as the function $F(z)$ in Eq. (7). Then, using Eqs. (2)–(7), we obtain a zero-order frozen wave for each intensity profile. Afterwards, the frozen waves evaluated at $z = 0$ are added together to obtain the complex light-sheet hologram. The phase in this case arises naturally from the addition of all the individual Bessel beams that reproduce the target intensity profile [46]. The approach can be further extended to reproduce 3D scenes, as shown in Fig. 2.b), where each layer of the scene generated in this manner is referred to as a holographic light sheet. This enables the projection of a target field in a plane parallel to the direction of light propagation, in contrast to conventional holography methods that primarily reproduce target fields perpendicular to this direction, as presented in Fig. 2.c).

A hologram $H(x, y)$ that reproduces a target scene composed of light sheets is obtained by evaluating the field $\Psi(\rho, z, t)$ at the hologram plane $z = 0$. This procedure results in a complex-valued hologram, as shown in Fig. 3.a). Since we are interested in reproducing the light sheets using a binary amplitude modulator (BAM), we must encode the complex hologram into a BAH. The first step in this encoding process is to convert the complex hologram into an amplitude-only hologram $H_a(x,y)$, which is obtained by taking its real part:

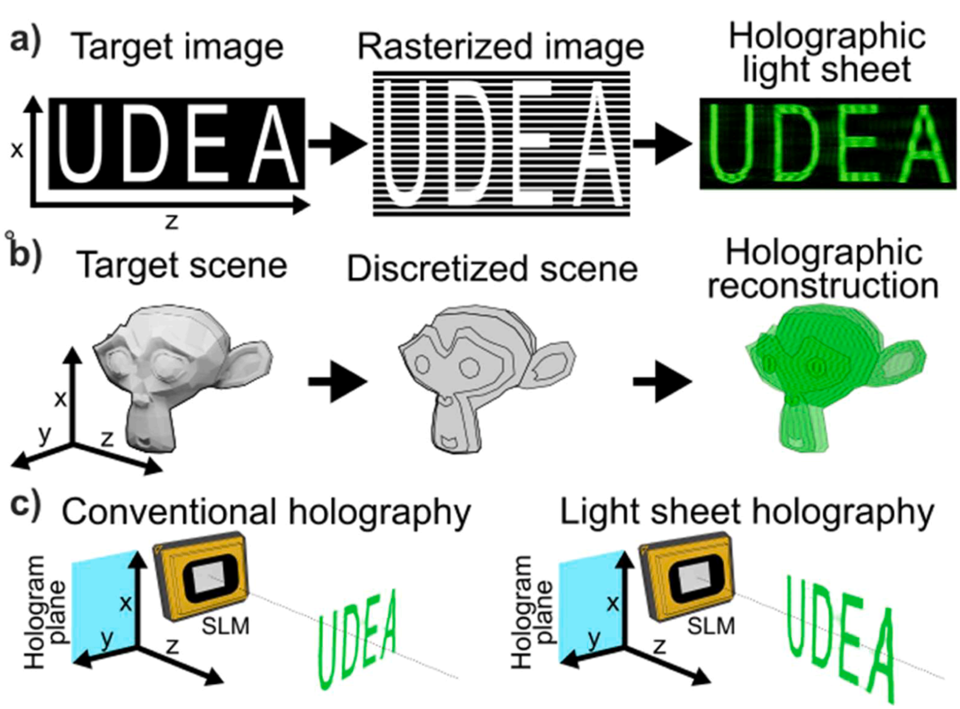

Fig. 2. Reproduction of scenes using frozen waves. a) Images are discretized, row by row, and each row is reproduced using frozen waves to produce a holographic light sheet. b) 3D scenes are discretized into layers, and each layer is reproduced using holographic light sheets. c) Light sheet reconstructions are oriented perpendicular to the hologram plane, in contrast to conventional holography reconstructions, which are parallel to the hologram plane. SLM: Spatial light modulator.

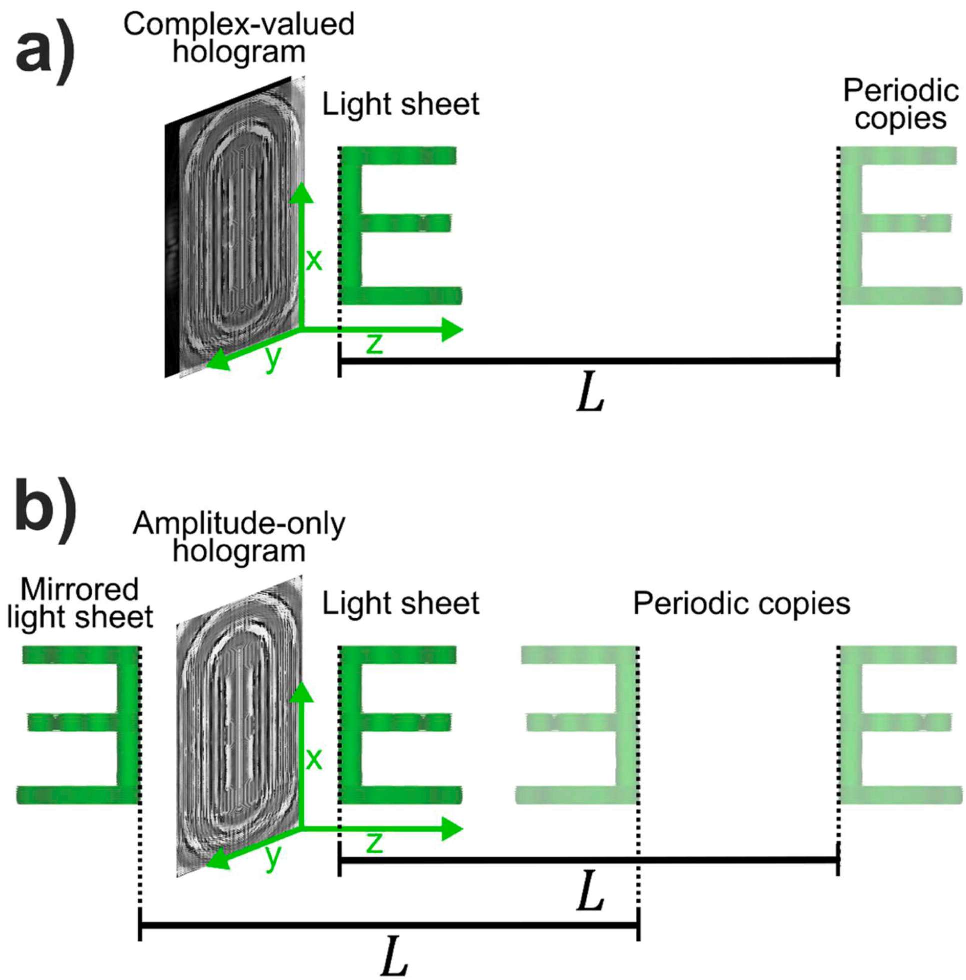

Fig. 3. Reconstruction of a holographic light sheet using a) the complex hologram and b) the amplitude-only hologram. ***L***: extension of the frozen waves composing the light sheets.

$$H_a(x,y) = \mathrm{Real}(H(x,y)). \tag{8}$$

The resulting hologram reproduces the light sheets within the longitudinal interval $[0,L]$, together with a mirrored version in the interval $[-L,0]$. Furthermore, both versions have periodic replicas with a period L. Given this configuration, the periodic replicas of the mirrored light sheet could interfere with the desired reconstruction. To avoid this issue, we restrict the size of the scene to the interval $[0,L/2]$. This ensures that the periodic replicas of the original scene and its mirror image are generated in non-overlapping, alternating regions, as depicted in Fig. 3. b).

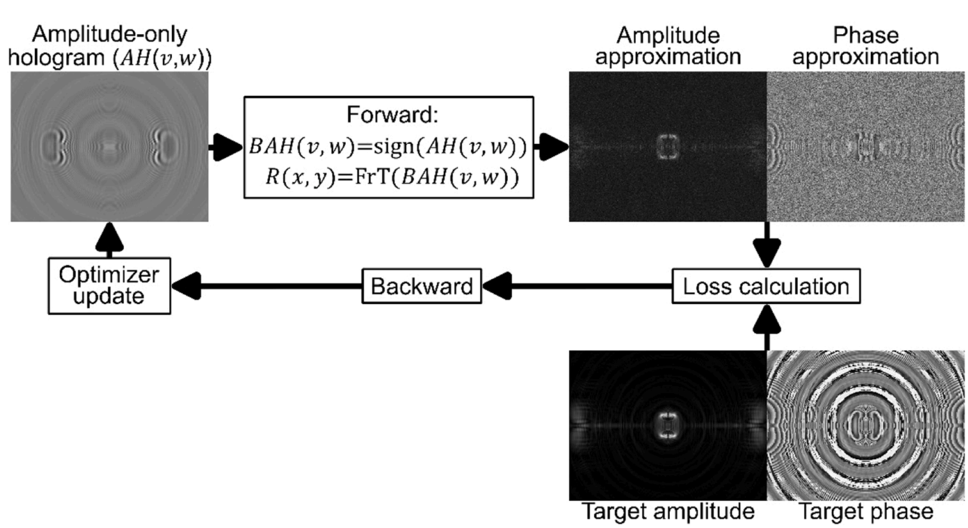

Fig. 4. Flowchart of an iteration of B-SGD. $BAH(v,w)$: Binary amplitude hologram, $R(x,y)$: hologram reconstruction, FrT: Fresnel transform.

The amplitude-only hologram can be further encoded into a BAH through binarization; however, direct binarization introduces substantial quantization noise that hinders reconstruction quality. To address this issue, we propose a binary-stochastic gradient descent (B-SGD) optimization scheme that employs complex loss functions. B-SGD is an iterative algorithm that minimizes the discrepancy between the target and reconstructed fields, as quantified by a selected loss function.

The flowchart of a single iteration of the B-SGD algorithm is shown in Fig. 4. The algorithm optimizes the amplitude-only hologram to minimize the quantization noise introduced by binarization. Specifically, in each iteration, the hologram is binarized and then propagated through free-space to a selected plane, a process modeled by a Fresnel transform (FrT). At this plane, the chosen loss function between the reconstructed field and the target is evaluated, the gradient of this loss with respect to the hologram is computed, and the amplitude-only hologram is updated using stochastic gradient descent with the Adam optimizer [57]. The target field used during this optimization is obtained by propagating the initial amplitude-only hologram prior to binarization to the selected plane. It is important to note that the binarization operator is non-differentiable. Therefore, for gradient computation, it is approximated by a hard hyperbolic tangent function, defined as $\mathrm{Htanh}(x) = \max(-1, \min(1, x))$.

Traditional implementations of B-SGD optimization employ loss functions that only measure the difference between the intensity of the reconstruction at a given plane and a target 2D intensity distribution. An example of these loss functions is the mean squared error (MSE), defined between two images A and B as

$$\mathscr{L}_{\mathrm{MSE}}(A,B) = \frac{1}{MN}\sum_{i,j}^{M,N}\left(A[i,j] - B[i,j]\right)^2, \tag{9}$$

where $M \times N$ is the resolution of the images, and i and j denote individual pixels. This approach can be extended to reproduce 3D intensity distributions by evaluating loss functions at multiple planes; however, this method only optimizes the distribution at discrete planes and demands an increasingly large computation time as the number of evaluated planes grows. These characteristics make the method especially inefficient when reconstructing holographic light sheets, which produce a continuous intensity distribution over a large longitudinal interval. To solve this issue, we propose the use of a complex loss function that evaluates the entire complex field at a single plane, thus optimizing the entire 3D optical field. This is because the optical field at a single plane determines its subsequent evolution upon propagation [53].

In this work, we employ a complex loss function based on the MSE metric. We propose the complex mean squared error loss ($\mathscr{L}_{\mathrm{CMSE}}$) function given by

$$\mathscr{L}_{\mathrm{CMSE}} = \mathscr{L}_{\mathrm{MSE}}(\mathrm{Real}(T),\ \mathrm{Real}(R)) + \mathscr{L}_{\mathrm{MSE}}(\mathrm{Imag}(T),\ \mathrm{Imag}(R)), \tag{10}$$

where T denotes the target field, R is the reconstruction, and the functions $\mathrm{Real}(x)$ and $\mathrm{Imag}(x)$ return the real and imaginary parts of their complex arguments, respectively. In this manner, the algorithm optimizes a BAH to reproduce an entire scene composed of holographic light sheets by evaluating the loss function at a single plane, thereby reducing the computational cost compared with traditional optimization schemes. We now summarize our proposal as follows: Eqs. (2)-(7) are used to reproduce target scenes via holographic light sheets, which results in a complex-valued hologram. This hologram is then converted into an amplitude-only hologram using Eq. (8), and subsequently, B-SGD optimization with the $\mathscr{L}_{\mathrm{CMSE}}$ function is used to encode the target scene's light sheets into a BAH.

3. Numerical results

We first validated the proposed method by generating BAHs that reproduce a two-dimensional target scene using a holographic light sheet. The light sheet was composed of 86 frozen waves with an extension L of 90.0 cm and separated from each other by 32.4 μm. Each frozen wave was generated at a wavelength $\lambda = 640$ nm, using a central wavevector $Q = 0.999929\,k$, which determines the remaining parameters in accordance with Eqs. (3)-(7). The target scene was recovered within the longitudinal interval [19.0 cm, 40.0 cm]. The same scene was reproduced using the initial complex hologram, the corresponding amplitude-only hologram before binarization, and the BAHs obtained by binarizing this corresponding hologram using both direct binarization and our proposed B-SGD method with complex loss functions. For the optimization, the target complex field was obtained by propagating the original (non-binarized) complex hologram to a plane at a distance z_0 of 19.0 cm. Here, z_0 denotes the distance along the light propagation axis between the hologram plane and the closest notable feature of the reconstructed light sheet. The holograms that reproduce the light sheet have a resolution of 2048 × 2048 pixels and a pixel size of 5.4 μm. Unless stated otherwise, all holograms generated in this work for numerical tests share these specifications and all instances of B-SGD optimization were performed applying 200 iterations of the algorithm utilizing an NVIDIA RTX 2000 ADA. The B-SGD optimization process required approximately 29.6 s.

Fig. 5 shows the target scene and the reconstruction obtained from each light-sheet hologram. Since holographic light sheets are generated in planes parallel to the direction of propagation, the corresponding reconstructions are obtained by recording the intensity over the transverse area at different planes and digitally combining the results. As shown in the figure, the conversion from the complex hologram to an amplitude-only hologram does not introduce any notable degradation, and the optimized BAH provides significantly higher reconstruction quality than direct binarization, whose reconstruction presents loss of low-frequency content and severe edge artifacts compared to the original light sheet.

To quantify the performance of the optimization algorithm, we evaluated the correlation coefficient (CC) between the reconstructions and the target image, displaying the resulting values below each reconstruction. The correlation coefficient between two images A and B, of resolution $M \times N$, is defined as

$$\mathrm{CC}(A,B) = \frac{\sum_{i,j}^{M,N}(A[i,j] - \overline{A})(B[i,j] - \overline{B})}{\sqrt{\left(\sum_{i,j}^{M,N}(A[i,j] - \overline{A})^2\right)\left(\sum_{i,j}^{M,N}(B[i,j] - \overline{B})^2\right)}}, \tag{11}$$

where $\overline{A}$ and $\overline{B}$ denote the respective mean values, and i and j represent the individual pixels. This metric yields values between 0 and 1, where higher values indicate greater similarity between images. The behavior of the CC is consistent with the visually observed improvements, with the optimized BAH achieving a substantially higher CC than direct binarization. Moreover, the highest CC corresponds to the reconstruction from the amplitude-only hologram, which is used as the target field during optimization and thus serves as an upper bound on the achievable reconstruction quality.

We then evaluated the performance of the algorithm as a function of the propagation distance z_0. For this analysis, we used frozen waves with an extension L of 120.0 cm to generate light sheet holograms that reproduce an image of the letter A in the longitudinal interval $[z_0,\ z_0 + 7.0\ \mathrm{cm}]$. We then applied the proposed optimization scheme to convert the resulting holograms to BAHs. Figure 6 shows the CC between the target image and the reconstruction from each hologram as a function of the distance z_0. As expected, the CC is highest for the non-binarized holograms across all propagation distances. In contrast, direct binarization of the amplitude-only holograms consistently introduces considerable noise that results in low quality reconstructions with CC values between 0.2 and 0.4, approximately. B-SGD optimization does not produce significant enhancements when the propagation distance is too small. The improvement begins once the propagation distance z_0 exceeds approximately 10.0 cm and its effectiveness increases

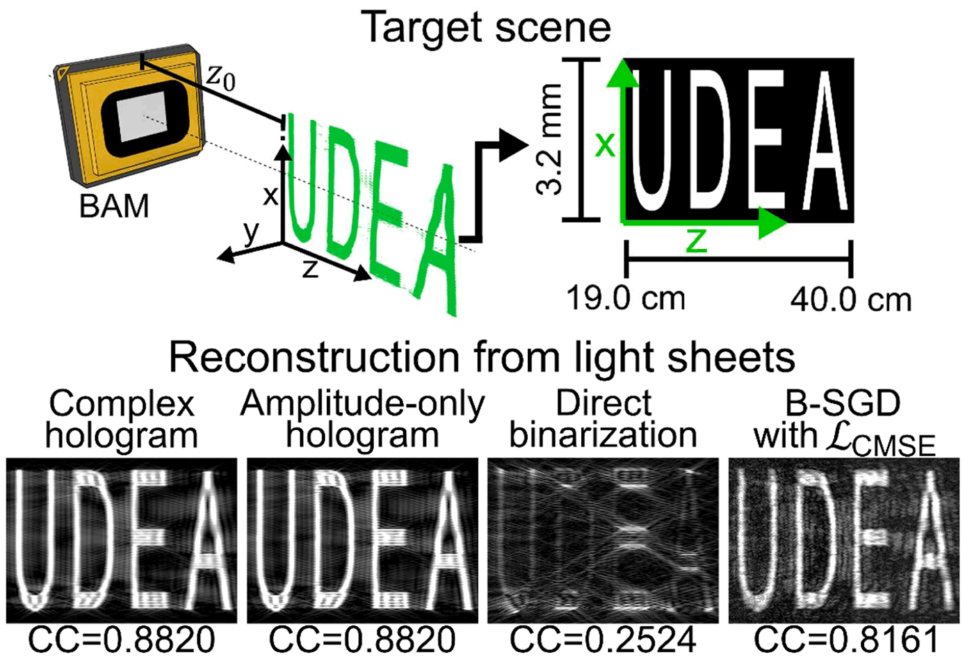

Fig. 5. Numerical results obtained using the proposed method to reconstruct an image using holographic light sheets. BAM: binary amplitude modulator, CC: correlation coefficient, $\mathbf{z}_0$: propagation distance between the hologram plane and the beginning of the reconstructed image.

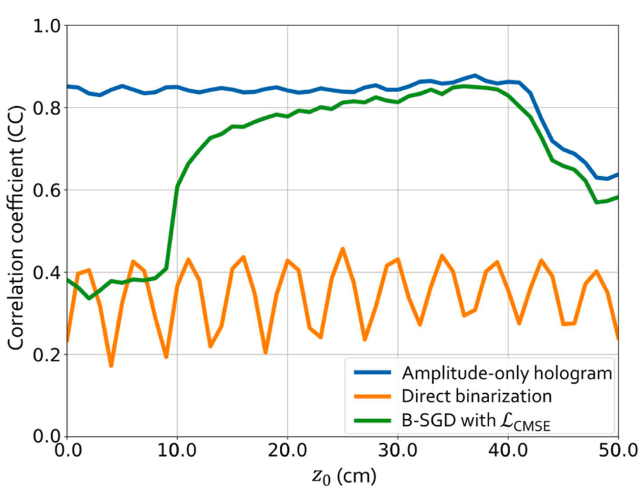

Fig. 6. Correlation coefficient between the reconstructed and target images as a function of the distance $\mathbf{z}_0$.

with greater distances. Finally, a sudden drop in reconstruction quality is observed for both the amplitude-only and optimized BAHs when the propagation distance z_0 surpasses approximately 40.0 cm. This is due to the finite size of the holograms, which limits the distance where the intensity profile can be controlled using frozen waves, regardless of the extension L. Overall, the optimization is most effective when the reconstructed image is located in the interval [10.0 cm, 40.0 cm].

The target image and the reconstructions obtained during this test for different propagation distances z_0 (5.0 cm, 25.0 cm, and 45.0 cm), along with the corresponding CC values, are shown in Figure 7. Consistent with the CC trend, all BAHs produce low-quality reconstructions at short distances. In contrast to direct binarization, the optimized BAH yields an evident improvement when the reconstructed image is positioned within the interval [10.0 cm, 40.0 cm]. Finally, when the distance z_0 exceeds 40.0 cm, the amplitude-only hologram produces a distorted reconstruction of the target image, which is observed in the results obtained from the corresponding BAHs.

The amplitude-only holograms provide reconstructions of nearly constant quality within the interval [0.0 cm, 40.0 cm]. In contrast, optimized BAHs yield inadequate reconstructions for scenes at distances below 10.0 cm, while achieving better results for scenes at greater distances within the interval [10.0 cm, 40.0 cm]. This behavior is caused by the dynamic range (DR) of the amplitude-only holograms. The DR refers to the ratio between the highest and lowest values present in a hologram. It is measured in decibels, and it is defined as

$$\mathrm{DR} = 10\log\left(\frac{P_2}{P_1}\right), \tag{12}$$

where P_2 and P_1 are the highest and lowest intensity values, respectively. Holograms with a high DR contain large variations in amplitude, requiring multiple degrees of freedom to be represented accurately. Since BAHs provide only two available amplitude states, reproducing holograms with a high DR is inherently challenging. Conversely, holograms with lower DR can be converted into a BAH with adequate results.

Fig. 8 presents the DR of the amplitude-only holograms from the previous test for each propagation distance. The DR is high at short propagation distances and tends to decrease as the distance increases. Here, we recall the results shown in Figs. 6 and 7, where the quality of the holograms after binarization deteriorates sharply for propagation distances z_0 below 10 cm. These observations suggest that the relationship between dynamic range (DR) and reconstruction quality after binarization is not linear. Instead, the results indicate the presence of an effective DR threshold at approximately 38 dB, above which the B-SGD procedure cannot adequately encode the amplitude information into a binary amplitude hologram (BAH). Conversely, below this threshold, further reductions in DR do not appear to produce significant variations in the overall reconstruction quality, as illustrated in Fig. 6.

To further demonstrate the capability of the method, we applied the proposed approach to reproduce a multiplane scene via holographic light sheets. We defined a scene composed of two adjacent light sheets, each reproducing an independent target image and separated by approximately 2.2 mm. The complex hologram corresponding to each light sheet is generated individually following the procedure described in the previous tests. These individual holograms are added to obtain the multiplane light-sheet hologram. This composite hologram is

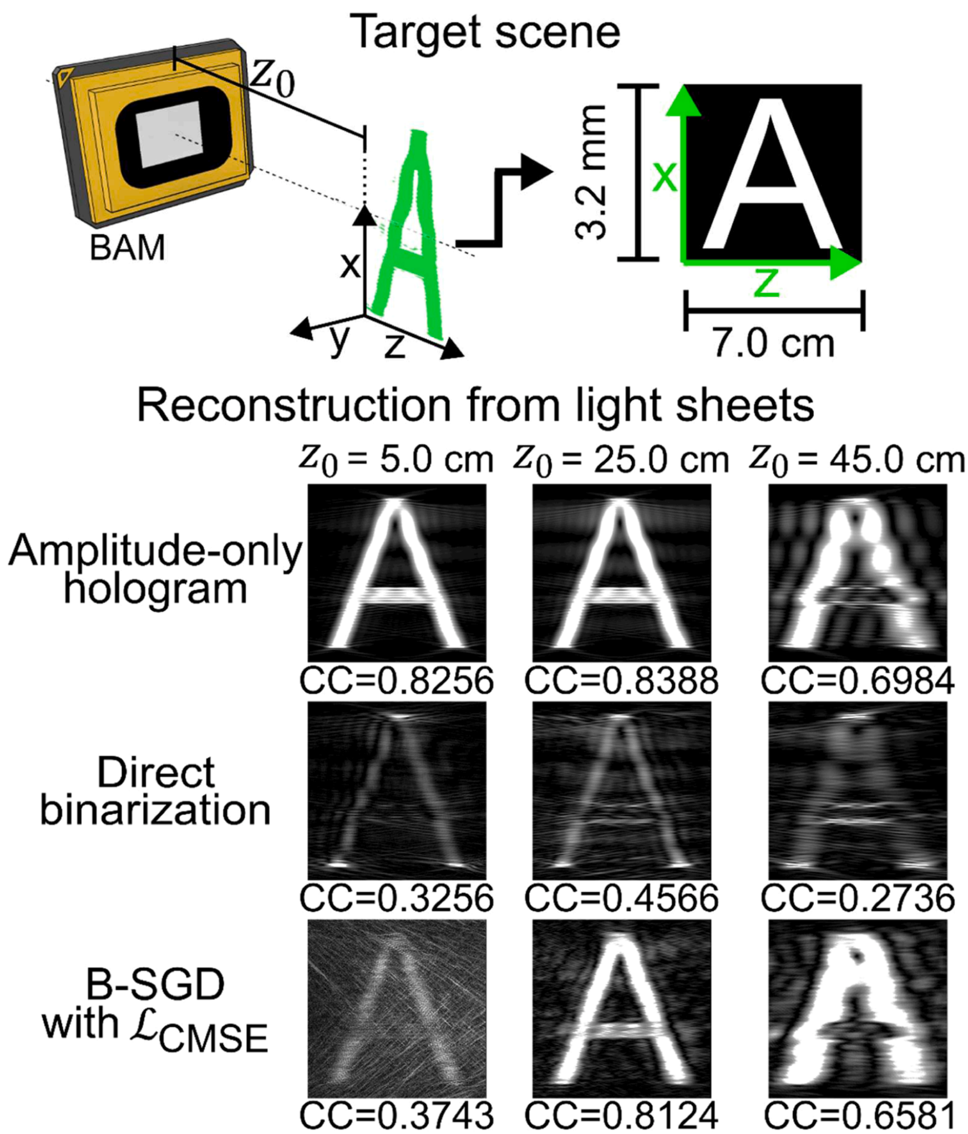

Fig. 7. Numerical results obtained using the proposed method to reconstruct an image using light sheets for different distances z_0. BAM: Binary amplitude modulator, CC: correlation coefficient, z_0: propagation distance from the hologram plane and the beginning of the reconstructed image.

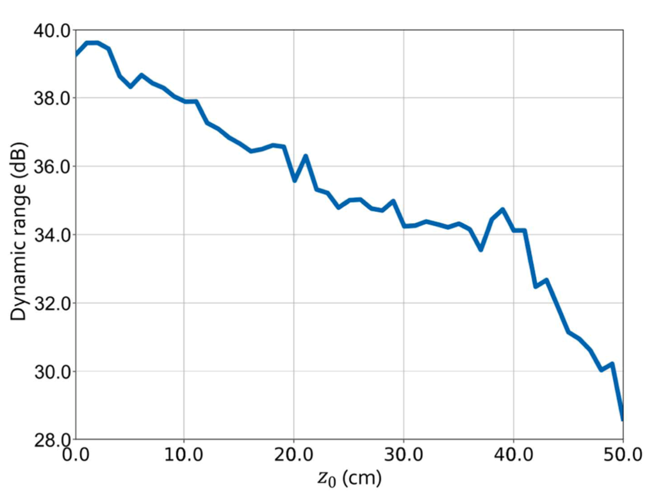

Fig. 8. Dynamic range of the holographic light sheets obtained using the proposed method to reconstruct an image of the letter A as a function of the distance z_0.

subsequently converted into a BAH using direct binarization and our proposed approach. In Fig. 9, we show the reconstructions of these light sheets from the initial amplitude-only hologram, the BAH obtained by direct binarization, and the BAH obtained using our proposed method. In each of these cases, the intensities of the two reconstructed light sheets are shown at their respective positions. As in previous tests, B-SGD optimization substantially improves the reconstruction quality compared to direct binarization. Furthermore, crosstalk between the two light sheets is negligible, and each object is reconstructed without noticeable traces of the other.

Despite this lack of crosstalk, compared to the results in Fig. 5, the presence of the field corresponding to the second light sheet interferes with the "UDEA" image, reducing the fidelity of the reconstruction. As reflected by the lower overall CC value, this behavior is consistent with the trend shown in Figs. 6 and 7.

One of the main reported advantages of light sheet holography over conventional layer-based holography is its ability to enable smaller interlayer distances while maintaining lower crosstalk. To verify if this advantage holds under binary amplitude modulation, we perform the following test: we generated a phase-only, layer-based multiplane hologram of the same two objects used in Fig. 9 via 2000 iterations of

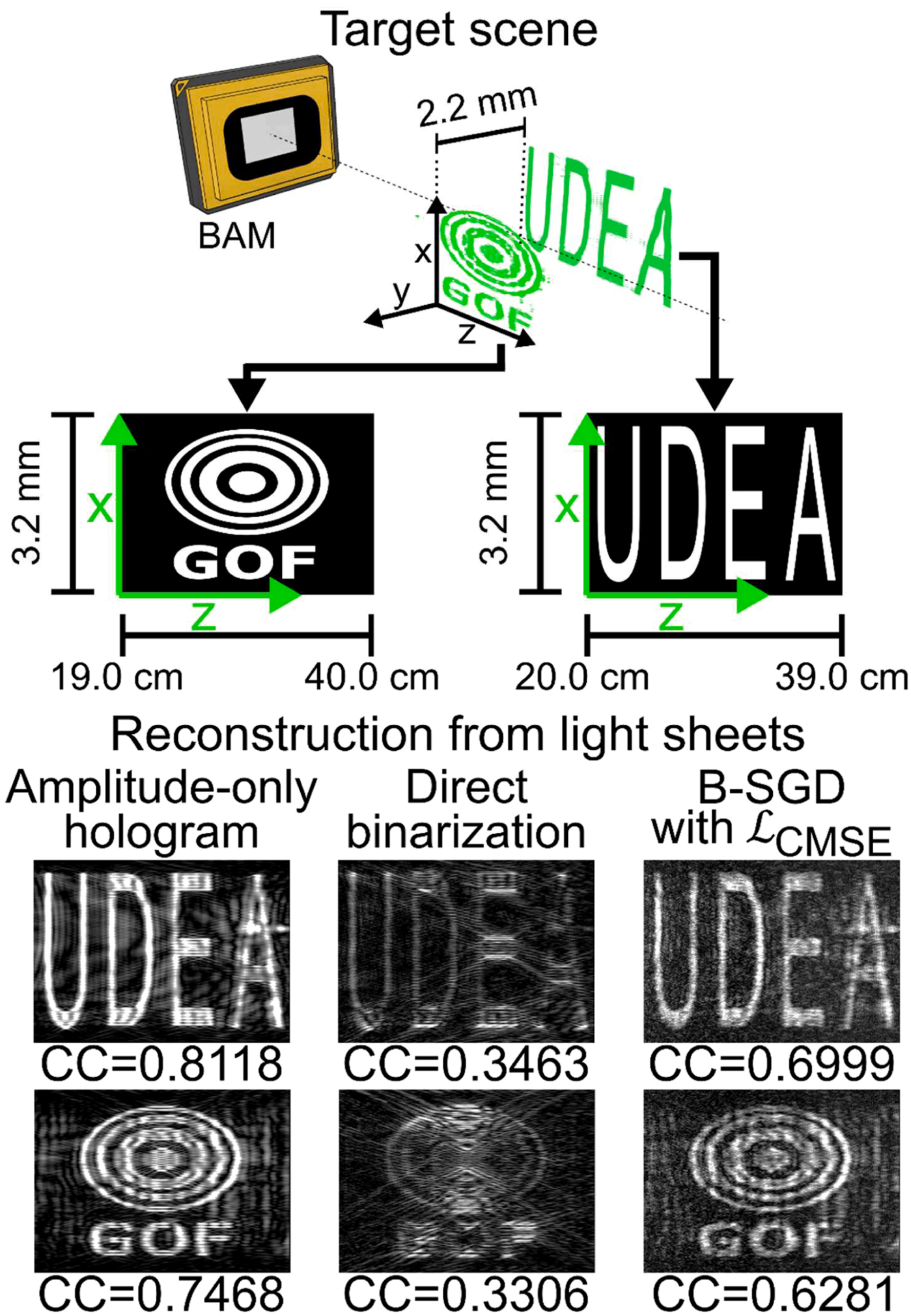

Fig. 9. Numerical results obtained using the proposed method to reconstruct a multiplane scene using holographic light sheets. BAM: Binary amplitude modulator, CC: correlation coefficient.

Wirtinger holography [35]. The two objects were oriented perpendicular to the propagation direction, separated by 2.2 mm, and starting at a distance $z_0 = 19.0$ cm from the hologram plane (Fig. 10). This hologram was then converted into a BAH using B-SGD optimization with the $\mathscr{L}_{\mathrm{CMSE}}$ function. Then, we compare the objects reconstructed from this binary hologram with those reconstructed from the BAH of the same two objects as light sheets shown in Fig. 9.

As observed in the results, when focusing on the plane containing the "UDEA" object, the conventional layer-based method provides higher reconstruction quality compared to the light sheet approach. However, it also has significant crosstalk from the "GOF" object due to the close distance between layers. The same effect occurs when comparing the plane where the "GOF" object is in focus in the layer-based reconstruction, where this object presents improved quality but severe crosstalk with the "UDEA" object. To quantify this crosstalk, we calculated the cross-correlation coefficient (CCC) between each reconstruction and the corresponding target image. These values are displayed below each reconstruction. The significantly lower CCC values demonstrate that holographic light sheets produce lower crosstalk between neighboring reconstructions. This property enables the reproduction of 3D and multiplane scenes with a smaller separation between layers.

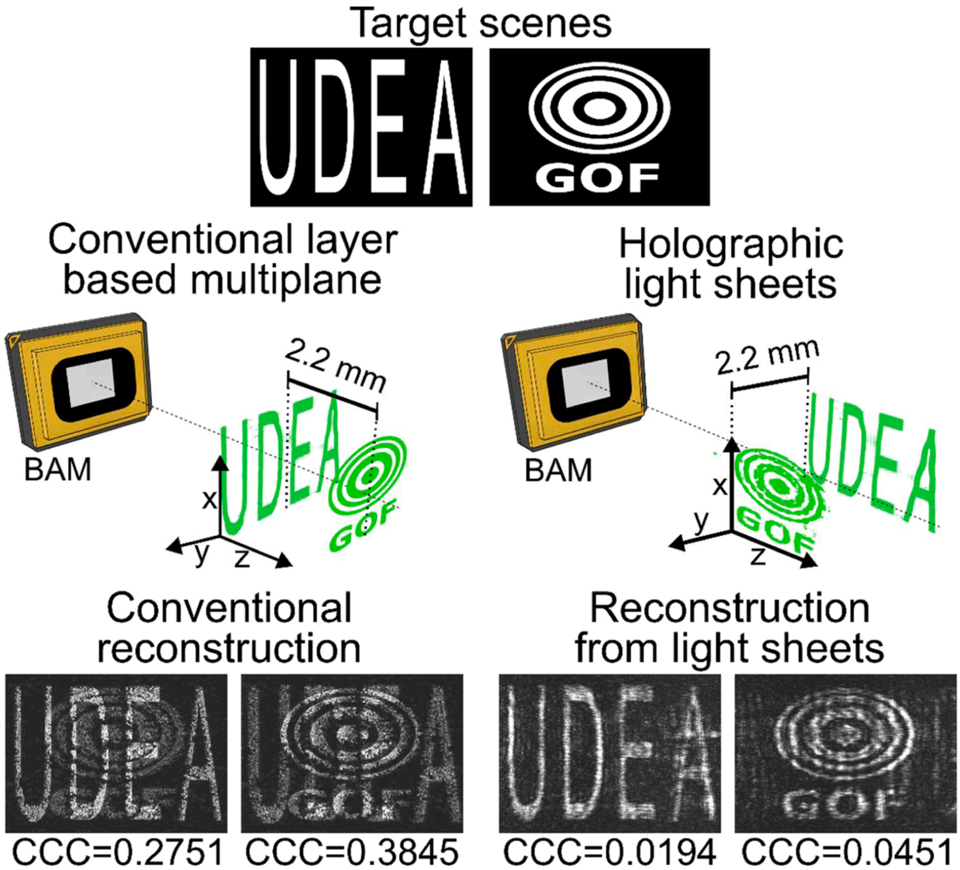

Fig. 10. Numerical results reproducing a multiplane scene composed of two images via holographic light sheets and conventional layer-based holography using BAHs. BAM: Binary amplitude modulator, CCC: cross-correlation coefficient.

4. Experimental results

To further evaluate the proposed method, we performed experimental tests using the setup shown in Fig. 11. Prior experimental implementations of light-sheet holography have been limited to phase-only SLMs. Our method, which encodes complex-valued holograms into BAHs, enables experimental reconstruction with a high-speed, low-cost BAM. Specifically, we employed a digital micromirror device (DMD, model DLPLCR50XEVM) as the BAM, with a resolution of 2048 $\times$ 1200 pixels and a pixel size of 5.4 μm. The system used a Shanghai Dream Lasers SDL-671-LN-100T (671 nm) as the light source. The output beam is expanded and collimated to produce a plane wave. The collimated beam is reflected by a mirror towards the DMD, which behaves as a blazed grating with a 12° tilt angle, corresponding to the rotation of the micromirrors between their resting and "on" states. The illumination beam impinges on the DMD at an angle selected to ensure the reflected

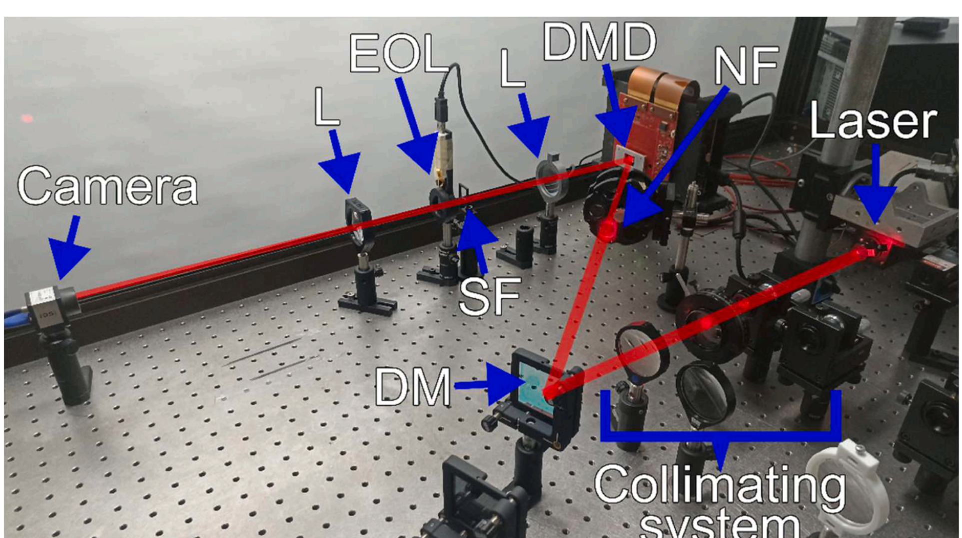

Fig. 11. Experimental setup. DMD: Digital micromirror device, L: lens, EOL: electro-optic lens, DM: dichroic mirror, NF: neutral filter, SF: spatial filter.

first diffraction order is perpendicular to the DMD surface. The modulated beam propagates through a 4f system, consisting of two lenses, each with a focal length of 20 cm. In the focal plane of the first lens a spatial filter removes the non-diffracted light. Finally, an electro-optic lens (Optotune EL-16–40-TC-VIS-5D-C) changes the plane of focus, and a camera IDS U3–3800CP-C-H (5536 × 3692 pixels, pixel size of 2.4 μm) records the reconstructions. The recorded images are digitally combined to recover the experimental light sheets. A neutral filter controls the intensity of the reconstruction.

Fig. 12 presents the experimental results obtained using the proposed method to reproduce a light sheet with BAHs. The holograms generated for the experimental tests had a resolution of 2048 × 1200 pixels to match that of the DMD. A total of 490 images were taken over the span of approximately 2 min while changing the focus of the electro-optic lens to scan the entire reconstruction range of the projected light sheets. Then, the entire light sheet was digitally assembled from the acquired images. The experimental reconstructions exhibit higher noise levels than their numerical counterparts but demonstrate the same overall trend, where direct binarization yields a low-quality reconstruction with some edges appearing especially bright, whereas B-SGD optimization produces a higher quality reconstruction. However, the increased brightness of the edges from direct binarization is less pronounced than in the numerical results. This can be attributed to the pupils of the lenses, which filter out high spatial frequencies. The higher noise levels compared to simulations, which are common to all experimental results, can be attributed to imperfections in the optical system and the recording process.

Fig. 13 presents the experimental reconstruction of the same multiplane scene of Fig. 9. Consistent with the numerical results, B-SGD optimization yields higher-quality reconstructions than direct binarization. The experimental results show less pronounced edge brightening for direct binarization, a consequence of high-frequency filtering by the spatial filter and lens pupils. Furthermore, the reconstruction exhibits the expected distance-dependent degradation, most evident in the letter "A" of the "UDEA" image, which corresponds to its lower CC value. These experimental results collectively validate the numerical findings and confirm the effectiveness of our B-SGD optimization for practical DMD-based projection.

5. Conclusions

We propose a method to generate BAHs for reconstructing bidimensional and multiplane scenes using light sheet holography, suitable for projection with binary amplitude modulators such as DMDs. This approach is based on an optimization scheme in the Fresnel domain that employs complex loss functions. Unlike traditional methods, which optimize 2D intensity distributions at discrete planes by evaluating an intensity-based loss at each plane, our method evaluates a complex loss function at a single plane to optimize the reconstruction of a continuous three-dimensional light field. Numerical simulations and experimental results validate the effectiveness of the optimization, demonstrating improved reconstruction quality across a wide range of distances from the hologram plane.

The generated BAHs reproduce holographic light sheets and their mirrored version with a periodicity equal to the longitudinal extension of the frozen waves that compose them. As a result, the target scenes must be confined to half the extension of the frozen waves to avoid superposition with the mirrored light sheet. Additionally, we evaluated the effect of propagation distance during optimization. The scheme produces notable improvements for scenes reconstructed at distances between 10.0 cm and 40.0 cm, with a higher effectiveness for larger values within this range. This behavior is due to the progressive reduction of the hologram's dynamic range for scenes reconstructed at greater propagation distances, thereby facilitating binarization. The sudden drop in quality for scenes reconstructed at distances beyond 40.0 cm is due to the finite size of the holograms, which limits the maximum distance at which the intensity profile can be controlled using frozen waves.

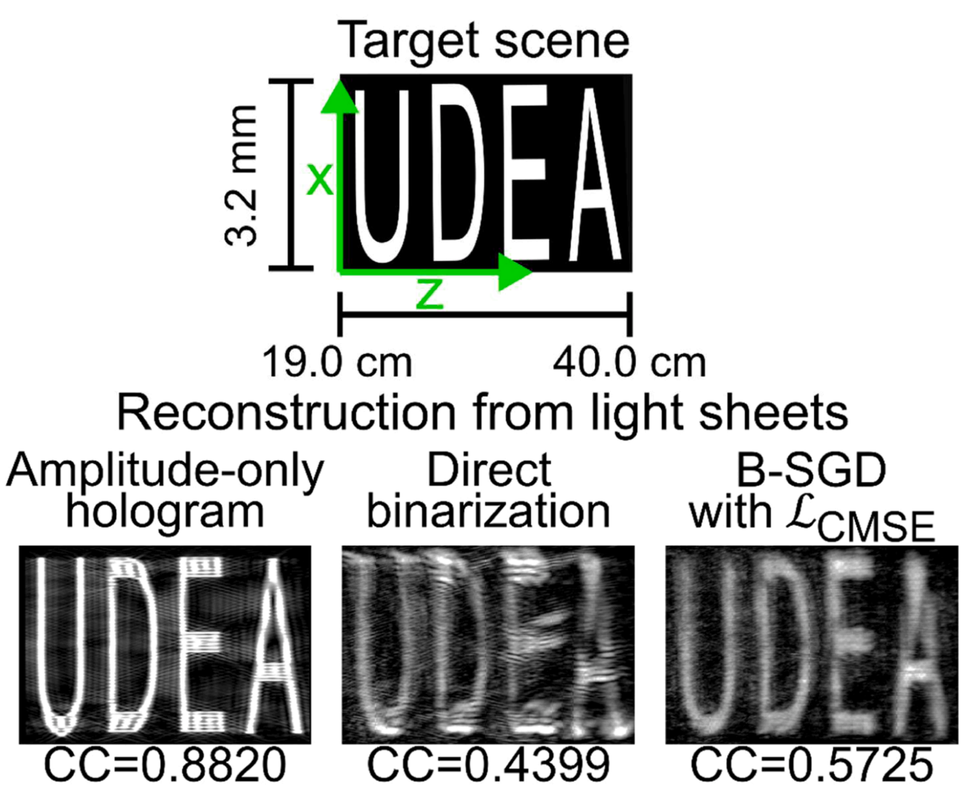

Fig. 12. Experimental results obtained using the proposed methods to reconstruct an image using holographic light sheets converted to binary amplitude holograms. CC: Correlation coefficient.

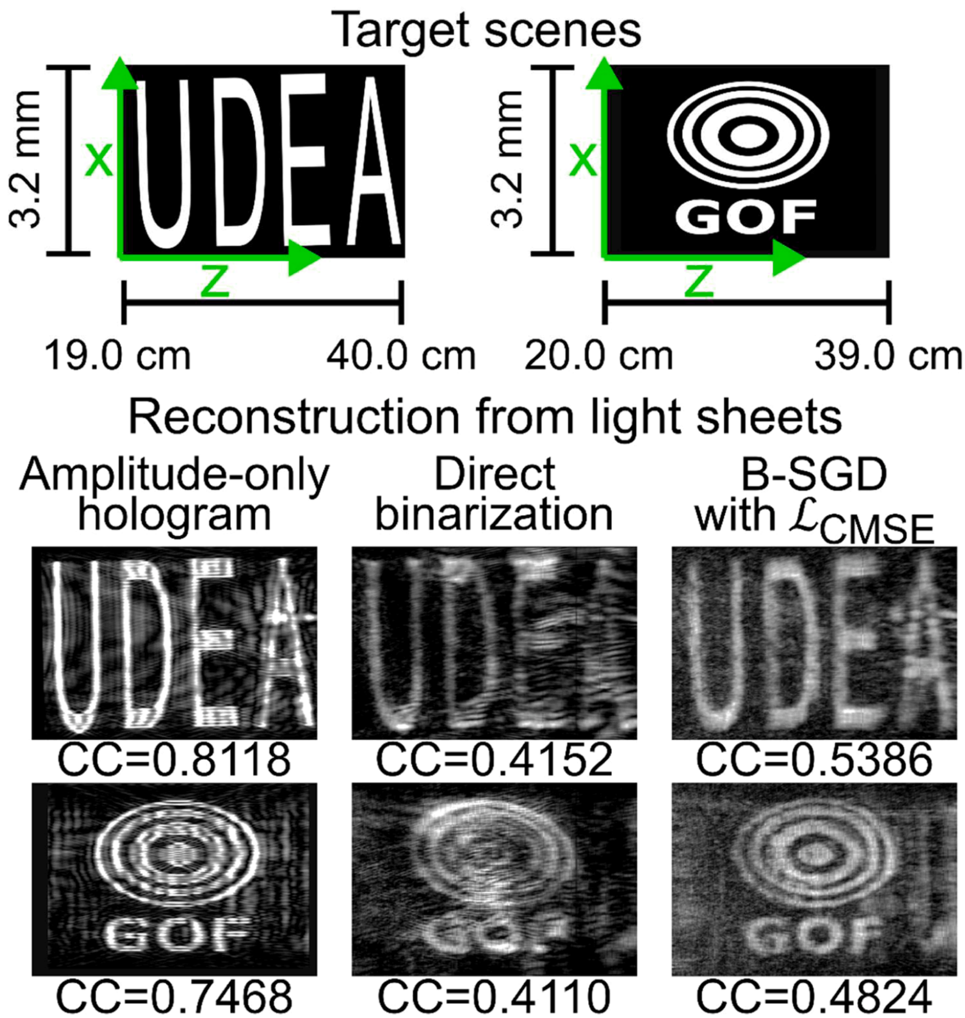

Fig. 13. Experimental results obtained using the proposed methods to reconstruct a multiplane scene with light sheet holograms. CC: Correlation coefficient.

Numerical and experimental results demonstrate that, compared with traditional layer-based holography, reconstructions using light sheets permit a smaller separation distance between planes in multiplane scenes while maintaining lower crosstalk. They also allow for uniform sampling, in contrast to layer-based approaches, which require larger separation distances as the distance to the hologram plane increases. These properties, along with other attractive characteristics, namely self-healing and attenuation resistance, make using BAHs to reproduce light-sheet-based scenes an attractive proposal. Likewise, the ability to generate frozen waves with BAHs enables the use of DMDs to investigate and implement advanced applications, such as optical tweezers, atom guides, and optical scalpels. The integration of DMDs leverages the advantages of these modulators, such as the higher refresh rate, which is especially advantageous for dynamic applications. Furthermore, the success of the optimization scheme to reproduce these high-complexity structured fields also suggests its broader applicability for projecting other types of scenes with DMDs.

Among the potential research directions for achieving further improvements in BAH generation and light-sheet projection is the design and evaluation of composite complex-valued loss functions that promote improved optimization convergence. For instance, this could involve combining a per-pixel loss function, such as $\mathscr{L}_{\mathrm{CMSE}}$, with additional terms that assess the global structure of the optical field. Another promising avenue is the tailoring of complex light sheet hologram generation parameters to enable more efficient conversion into BAH. This may include implementing a pre-optimization step to minimize amplitude variations in the complex hologram, thereby reducing the dynamic range and mitigating the limitations observed when binarizing light sheet holograms corresponding to scenes located at short propagation distances.

We believe BAH optimization with complex loss functions represents a powerful tool for harnessing the advantages of DMD modulation, effectively lowering the barrier to entry for a wide range of applications that require high-quality, cost-effective, and high-speed generation of 3D structured light.

Funding

Comité para el Desarrollo de la Investigación—CODI (Universidad de Antioquia—UdeA, Colombia); Sistema General de Regalías de Colombia (BPIN 2024000100091).

Data availability

Data underlying the results presented in this paper are not publicly available at this time but may be obtained from the authors upon reasonable request.

CRediT authorship contribution statement

Juan Andrés González-Moncada: Writing – review & editing, Writing – original draft, Visualization, Validation, Software, Methodology, Investigation, Formal analysis, Data curation, Conceptualization. **Alejandro Velez-Zea:** Writing – review & editing, Writing – original draft, Visualization, Validation, Supervision, Software, Resources, Project administration, Methodology, Investigation, Funding acquisition, Formal analysis, Data curation, Conceptualization. **John Fredy Barrera-Ramírez:** Writing – review & editing, Writing – original draft, Visualization, Validation, Supervision, Software, Resources, Project administration, Methodology, Investigation, Funding acquisition, Formal analysis, Data curation, Conceptualization.

Declaration of competing interest

The authors declare that they have no known competing financial interests or personal relationships that could have appeared to influence the work reported in this paper.

References

[1] Gabor D. A new microscopic principle. Nature 1948;161:777–8.
[2] Brown BR, Lohmann AW. Complex spatial filtering with binary masks. Appl Opt 1966;5:967–9.
[3] Lohmann AW, Paris DP. Binary Fraunhofer holograms, generated by computer. Appl Opt 1967;6:1739–48.
[4] Wang Y, Dong D, Christopher PJ, Kadis A, Mouthaan R, Yang F, Wilkinson TD. Hardware implementations of computer-generated holography: a review. Opt Eng 2020;59:102413.
[5] Sahin E, Stoykova E, Mäkinen J, Gotchev A. Computer-generated holograms for 3D imaging: a survey. ACM Comput Surv 2020;53:32.
[6] Bergmann RB, Kalms M, Falldorf C. Optical in-process measurement: concepts for precise, fast and robust optical metrology for complex measurement situations. Appl Sci 2021;11:10533.
[7] Xu K, Hu H, Zhang X, Wei H, Zhang Z, Zhang X. Accuracy verification methodology for computer-generated hologram used for testing a 3.5-meter mirror based on an equivalent element. Light Adv Manuf 2024;5:25.
[8] Zlokazov EY, Kolyuchkin VV, Lushnikov DS, Smirnov AV. Computer-generated holograms application in security printing. Appl Sci 2022;12:3289.
[9] Sun F, Zhu L, Wang W, Shi Z, Liu Y, Xu Y, Shi Q, Leng Y, Li R. Three-dimensional dynamic optical trapping using non-iterative computer-generated holography. Opt Lasers Eng 2023;164:107500.
[10] Blinder D, Birnbaum T, Ito T, Shimobaba T. The state-of-the-art in computer generated holography for 3D display. Light Adv Manuf 2022;3:35.
[11] González-Moncada JA, Velez-Zea A, Barrera-Ramírez JF. Multiplane experimental optical data encryption using phase only holography. Opt Lasers Eng 2025;188:108900.
[12] Zhang W, Nana Y, Ji X, Lu B, Hui X, Wang X, Xi S. Multi-key hybrid encryption optical codebook based on five-dimensional Hamiltonian conservative chaotic system. Opt Express 2025;33:18611–23.
[13] Han B, Zhao Y, Ji JH, Xu Z, Yin X, Qin XY. Full-color holographic encryption system using the hierarchical chaotic algorithm. J Opt Soc Am A 2025;42:A7–15.
[14] Shi L, Li B, Matusik W. End-to-end learning of 3D phase-only holograms for holographic display. Light Sci Appl 2022;11:247.
[15] Ren YX, Lu RD, Gong L. Tailoring light with a digital micromirror device. Ann Phys 2015;527:447–70.
[16] Zhuang Z, Ho HP. Application of digital micromirror devices (DMD) in biomedical instruments. J Innov Opt Health Sci 2020;13:2030011.
[17] Jaramillo-Osorio A, Bustamante-Quinchia S, Muñoz B, Velez-Zea A, Barrera-Ramírez JF, Torroba R. Experimental Fresnel and Fourier digital holography using a digital micro-mirror device. J Opt 2021;23:035701.
[18] Popoff SM, Gutiérrez-Cuevas R, Bromberg Y, Matthés MW. A practical guide to digital micro-mirror devices (DMDs) for wavefront shaping. J Phys Photonics 2024;6:043001.
[19] Tsang PWM, Poon TC. Novel method for converting digital Fresnel hologram to phase-only hologram based on bidirectional error diffusion. Opt Express 2013;21:23680–6.
[20] Shimobaba T, Wang F, Starobrat J, Kowalczyk A, Suszek J, Ito T. Comparison of double-phase hologram and binary amplitude encoding: holographic projection and vortex beam generation. Appl Opt 2023;62:7471–9.
[21] Chen L, Zhang H, Cao L, Jin G. Non-iterative phase hologram generation with optimized phase modulation. Opt Express 2020;28:11380–92.
[22] Peng Y, Choi S, Padmanaban N, Wetzstein G. Neural holography with camera-in-the-loop training. ACM Trans Graph 2020;39:185.
[23] Shimobaba T, Blinder D, Birnbaum T, Hoshi I, Shiomi H, Schelkens P, Ito T. Deep-learning computational holography: a review. Front Photonics 2022;3:854391.
[24] Choi S, Jang C, Lanman D, Wetzstein G. Synthetic aperture waveguide holography for compact mixed-reality displays with large étendue. Nat Photonics 2025;19:854–63.
[25] Ovchinnikov AS, Krasnov VV, Cheremkhin PA, Rodin VG, Savchenkova EA, Starikov RS, Evtikhiev NN. What binarization method is the best for amplitude inline fresnel holograms synthesized for divergent beams using the direct search with random trajectory technique? J Imaging 2023;9:28.
[26] Min K, Park JH. Quality enhancement of binary-encoded amplitude holograms by using error diffusion. Opt Express 2020;28:38140–54.
[27] Yang G, Jiao S, Liu JP, Lei T, Yuan X. Error diffusion method with optimized weighting coefficients for binary hologram generation. Appl Opt 2019;58:5547–55.
[28] Seldowitz MA, Allebach JP, Sweeney DW. Synthesis of digital holograms by direct binary search. Appl Opt 1987;26:2788–98.
[29] Liu JP, Tsai CM. Binary computer-generated holograms by simulated-annealing binary search. Photonics 2022;9:581.
[30] Yu ST, Luo A, Jiang L, Liu YF, Gong L, Yuan ZS. Direct binary search method for high-resolution holographic image projection. Opt Express 2022;30:26856–64.
[31] Lu C, Jin S, Hu X, Zhao X, Qi Z, Chen W, Cui Y. A region based random multi-pixel search algorithm to improve the binary hologram reconstruction quality. Opt Lasers Eng 2023;161:107322.
[32] Lee B, Kim D, Lee S, Chen C, Lee B. High-contrast, speckle-free, true 3D holography via binary CGH optimization. Sci Rep 2022;12:2811.
[33] Velez-Zea A, Hoyos-Peláez CA, Barrera-Ramírez JF. High-quality binary amplitude hologram generation for digital micromirror device based holographic display. Opt Lasers Eng 2025;191:108994.
[34] González-Moncada JA, Velez-Zea A, Barrera-Ramírez JF. Complex-to-binary amplitude hologram conversion using complex loss functions. Opt Express 2025;33:38963–83.
[35] Chakravarthula P, Peng Y, Kollin J, Fuchs H, Heide F. Wirtinger holography for near-eye displays. ACM Trans Graph 2019;38:213.
[36] Yang D, Seo W, Yu H, Kim SI, Shin B, Lee CK, Moon S, An J, Hong JY, Sung G, Lee HS. Diffraction-engineered holography: beyond the depth representation limit of holographic displays. Nat Commun 2022;13:6012.
[37] Zheng H, Wang Z, Peng J, Xia X, Yu Y. Multiplane full-color phase-only holograms generation based on iterative algorithm with a modified amplitude constraint. Displays 2023;79:102508.
[38] Kavaklı K, Itoh Y, Urey H, Akşit K. Realistic defocus blur for multiplane computer-generated holography. In: 2023 IEEE Conference Virtual Reality and 3D User Interfaces (VR); 2023. p. 418–26.
[39] Zamboni-Rached M. Stationary optical wave fields with arbitrary longitudinal shape by superposing equal frequency Bessel beams: frozen waves. Opt Express 2004;12:4001–6.
[40] Dorrah AH, Zamboni-Rached M, Mojahedi M. Generating attenuation-resistant frozen waves in absorbing fluid. Opt Lett 2016;41:3702–5.
[41] Suarez RAB, Ambrosio LA, Neves AAR, Zamboni-Rached M, Gesualdi MRR. Experimental optical trapping with frozen waves. Opt Lett 2020;45:2514–7.
[42] Suarez RAB, Neves AAR, Gesualdi MRR. Optical trapping with higher-order frozen waves. J Opt Soc Am B 2023;40:631–6.
[43] Dorrah AH, Palmieri A, Li L, Capasso F. Rotatum of light. Sci Adv 2025;11:adr9092.
[44] Corato-Zanarella M, Zamboni-Rached M. Electromagnetic frozen waves with radial, azimuthal, linear, circular, and elliptical polarizations. Phys Rev A 2016;94:053802.
[45] Dorrah AH, Rubin NA, Tamagnone M, Zaidi A, Capasso F. Structuring total angular momentum of light along the propagation direction with polarization-controlled meta-optics. Nat Commun 2021;12:6249.
[46] Dorrah AH, Bordoloi P, de Angelis VS, de Sarro JO, Ambrosio LA, Zamboni-Rached M, Capasso F. Light sheets for continuous-depth holography and three-dimensional volumetric displays. Nat Photonics 2023;17:427–34.
[47] Angelis VS, Dorrah AH, Ambrosio LA, Capasso F. Conformal holography with curved light sheets. Opt Express 2025;33:6567–80.
[48] de Angelis VS, Dorrah AH, Ambrosio LA, Miller DAB, Capasso F. Structuring light waves in 3D volumes with high precision using communication mode optics. Optica 2025;12:1502–13.
[49] Asoudegi N, Dorrah AH, Mojahedi M. Deep learning-assisted light sheet holography. Opt Express 2024;32:1161–75.
[50] Olarte OE, Andilla J, Gualda EJ, Loza-Alvarez P. Light-sheet microscopy: a tutorial. Adv Opt Photonics 2018;10:111–79.
[51] Hillman EMC, Voleti V, Li W, Yu H. Light-sheet microscopy in neuroscience. Annu Rev Neurosci 2019;42:295–313.
[52] Reis GB, Gesualdi MRR. Turbulence effects in frozen waves: experimental generation and analysis via holographic techniques. Opt Lett 2025;50:2097–100.
[53] Goodman JW. Introduction to Fourier optics. Roberts and Company publishers; 2005.
[54] Georgieva A, Belashov AV, Petrov NV. Optimization of DMD-based independent amplitude and phase modulation by analysis of target complex wavefront. Sci Rep 2022;12:7754.
[55] Goorden SA, Bertolotti J, Mosk AP. Superpixel-based spatial amplitude and phase modulation using a digital micromirror device. Opt Express 2014;22:17999–8009.
[56] Zamboni-Rached M, Mojahedi M. Shaping finite-energy diffraction- and attenuation-resistant beams through Bessel-Gauss-beam superposition. Phys Rev A 2015;92:043839.
[57] Kingma D.P., Ba J.L. Adam: a method for stochastic optimization. arXiv 2014; arXiv:1412.6980.